Journal of Biomedical Optics 8(4), 618–628 (October 2003)

Small-volume frequency-domain oximetry: phantom experiments and first *in vivo* results

Stefan Willmann
Albert Terenji
Jens Osterholz
Jörg Meister
Peter Hering
Heinrich-Heine University
Department of Laser Medicine
D-40225 Düsseldorf, Germany

Hans-Joachim Schwarzmaier
Klinikum Krefeld
Department of Applied Medical Technology
D-47805 Krefeld, Germany

Abstract. We describe a new method to determine the oxygen saturation and the total hemoglobin content of tissue *in vivo* absolutely at small source-detector separations (<10 mm). Phase and mean intensity of modulated laser light of various wavelengths was measured at several predetermined source-detector separations in the frequency domain. From these measured quantities, the absorption coefficient was derived using the modified time-integrated microscopic Beer-Lambert law (MBL). In addition, the interaction volume of the photons was determined using a multi-layer Monte-Carlo model of human skin. To evaluate the method, we employed homogenous solid phantoms (consisting of TiO_2 particles embedded in resin) with mean scattering and absorbing properties comparable to those of human skin. Furthermore, *in vivo* measurements were performed in a healthy volunteer to demonstrate that the technique is applicable for the determination of the oxygen saturation and the total hemoglobin content in the skin *in vivo*. The proposed technique is especially suited for the on-line determination of the oxygen saturation and total hemoglobin content in applications where small applicators are required (e.g., fetal oxygen monitoring *sub partu*). [DOI: 10.1117/1.1608892]

Keywords: frequency-domain spectroscopy; photon density waves; microscopic Beer-Lambert law; Monte-Carlo technique; tissue phantoms; oxygen saturation.

Paper 02028 received May 6, 2002; revised manuscript received Nov. 18, 2002; accepted for publication May 13, 2003.

1 Introduction

Tissue oximetry based on optical techniques has been performed since 1942.[1,2] The spectral range between 600 and 1000 nm is well suited for optical tissue oximetry because at these wavelengths, the absorption spectrum of hemoglobin is closely related to its oxygenation state.[2,3] Moreover, the penetration depth of biological tissues is high in this spectral range. Usually, the light attenuation ratio at two different wavelengths is measured. Measurements are performed in either transmission or reflection geometry depending on the part of the body accessible to the sensor of the pulse oximeter.[4–6] From these data, the oxygen saturation $S[O_2]$ can be derived. However, the measurement of a simple attenuation ratio does not account for the contributions of photon losses due to scattering within biological tissues. Thus, these systems do not provide absolute absorption data. Therefore, all systems available so far must be calibrated to account for scattering. To this end, the pulse-oximeter readings are usually compared with ex vivo blood samples measured by conventional blood gas analyzers.[6–8] Moreover, other absorbers such as melanin in the epidermal skin layer contribute to the background absorption and affect the measured quantities. Therefore, the latter cannot be taken into account without further calibration of the pulse oximeter. As a consequence, simple pulse oximetry reveals substantial errors when applied to different skin colors, for example, to Afro-Caribbean fetuses as reported by D'Antona et al.[9]

To overcome the need for calibration, quantitative methods have been developed to determine the absorption coefficient of a turbid medium *in vivo* absolutely such as, for example, the frequency-domain multi-distance (FDMD) method.[10–12] This technique is based on spatially resolved phase and intensity measurements using photon density waves in the frequency range of 10 to 100 MHz.[13–17] To derive the absorption coefficients from the measured quantities, the diffusion approximation of radiative transport theory is often employed.[15–17] Unfortunately, the diffusion approximation is only valid at large distances from the source (typically >20 mm in biological tissues).[18] Consequently, the applicators used in the framework of this technique are comparatively bulky and, therefore, are not suited for minimally invasive monitoring such as, e.g., that required for measuring fetal blood oxygen saturation *sub partu*. To describe the photon transport in areas close to the light source quantitatively, the Monte-Carlo technique has been employed[17] to extract the absorption coefficients from the measured quantities. However, Monte-Carlo simulations of photon transport in turbid media are currently still too time consuming to allow on-line processing of the measured data, although considerable progress has recently been made to accelerate the calculations.[19,20]

In this study, we propose to use the modified microscopic Beer-Lambert law (MBL) for the determination of the oxygen saturation and the total hemoglobin content for the first time. The modified MBL has been described previously[21] and is the first technique that allows for an absolute determination of the

1083-3668/2003/$15.00 © 2003 SPIE

absorption coefficient of turbid media at small source-detector separations on-line. Thus, the MBL can overcome the disadvantages of the techniques described above.

The aim of this study was to show that the MBL can be used to absolutely determine the oxygen saturation ($S[O_2]$) and total hemoglobin content (THC) on-line and *in vivo* at source detector separations suitable for minimally invasive applications such as the measurement of fetal oxygen saturation *sub partu*. To this end, a frequency-domain device was designed that was used in combination with the MBL for data processing. The system was evaluated *in vitro* using a series of solid scattering and absorbing phantoms with known optical properties mimicking those of neonate skin in the red and near-infrared spectral range. In addition, the influence of the layered skin structure and various contents of background absorber (e.g., melanin) on the oximeter readings has been investigated using the Monte-Carlo technique. Finally, a first *in vivo* feasibility test was performed to measure $S[O_2]$ and THC of blood in human tissue on the forearm of a healthy adult volunteer.

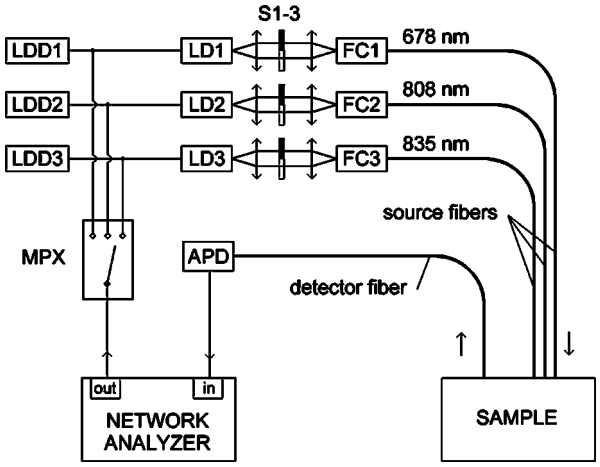

Fig. 1 Experimental setup of the frequency-domain spectrometer: LDD1–LDD3, laser diode drivers; LD1–LD3, laser diodes; S1–S3, shutters; FC1–FC3, fiber couplers; APD, avalanche photodiode; MPX, multiplexer.

2 Theory

To determine the absorption coefficient of biological tissue, we applied the microscopic Beer-Lambert law (MBL) first introduced by Tsuchiya and Urakami[22,23] in its modified time-integrated version.[21] The basic idea of the MBL is to apply the well-known Beer-Lambert law to the individual pathlengths of a photon that is multiply scattered in a turbid medium. The temporal impulse response function $R(\mu_a,\mu_s,t)$[22] depends on the scattering coefficient μ_s and the absorption coefficient μ_a and can be written as

$$R(\mu_s,\mu_a,t)=s(\mu_s,t)\exp\{-\mu_a c_n t\} \tag{1}$$

where $s(\mu_s,t)$ represents the probability of a scattered photon reaching the detector in the case of a non-absorbing medium ($\mu_a=0$). The term $\exp\{-\mu_a c_n t\}$ accounts for the losses due to absorption ($c_n=c_0/n$ is the phase velocity in the medium with refractive index n).

If the time-integrated intensity I_{DC} (in the following referred to as DC intensity)

$$I_{\mathrm{DC}}(\mu_s,\mu_a)=\int_0^\infty R(\mu_s,\mu_a,t)\,\mathrm{d}t \tag{2}$$

and the mean time of flight $\langle t\rangle$

$$\langle t\rangle=\frac{\int_0^\infty t\cdot R(\mu_s,\mu_a,t)\,\mathrm{d}t}{\int_0^\infty R(\mu_s,\mu_a,t)\,\mathrm{d}t} \tag{3}$$

of the photons are determined at two or more source detector separations, the absolute absorption coefficient μ_a can be derived from the slope of a $\ln\{I_{\mathrm{DC}}\}$ vs. $\langle t\rangle$ plot[21]:

$$\mu_a=-\frac{1}{c_n}\frac{\Delta\ln\{I_{\mathrm{DC}}\}}{\Delta\langle t\rangle}. \tag{4}$$

As discussed in detail in Ref. 21, Eq. (4) can be applied to turbid media with absorption coefficients between approximately 5×10^{-4} and 2 mm^{-1} and reduced scattering coefficients μ_s' between 0.2 and 2 mm^{-1}, a range typically found in biological tissues.[24–30] Outside this range of optical properties, the linear behavior of $\ln\{I_{\mathrm{DC}}\}$ as a function of $\langle t\rangle$ should no longer be assumed because of a weak dependence of I_{DC} and $\langle t\rangle$ on the scattering coefficient of the medium.

In the frequency domain, the mean time of flight can be determined from the slope of the phase (Φ) as a function of the frequency (f)[16]:

$$\langle t\rangle=\frac{\Delta\Phi}{2\pi\Delta f}. \tag{5}$$

As an analytical model, the MBL is suited to process the measured data on-line. Unlike the diffusion approximation, it is not limited to large source-detector separations. In addition, it has been shown to be insensitive to the measurement geometry.[31,32]

3 Experimental Methods

3.1 *Frequency-Domain Setup*

Frequency-domain measurements were performed using a setup similar to that described by Madsen et al.[33] A schematic drawing of the device is shown in Fig. 1. As light sources, three laser diodes were used [SDL 7432-H1 (λ=678 nm), SDL 2352-H1 (λ=808 nm), and SDL 5432-H1 (λ=835 nm), all from Spectra Diode Labs, San Jose, California]. The laser diodes were selectively bias-modulated in the frequency range between 300 kHz and 200 MHz by a vector network analyzer (HP 8712C, Hewlett Packard, Palo Alto, California) in combination with a high-frequency multiplexer (7016, Keithley, Cleveland, Ohio) and three bias tees (5580, Picosecond Labs, Boulder, Colorado). The modulated laser light was delivered to the sample via quartz/quartz optical fibers with a core diameter of 600 μm and a numerical aperture of 0.2. An identical fiber was used to collect the remitted photons at several source-detector separations ρ (between 3 and 9 mm). A high-speed avalenche-photodiode receiver (APD S90302C, EG&G Electrooptics, Boudreuil, Canada) with a spectral bandwidth of 800 MHz was used as optical detector. All measurements were performed with a frequency resolution of 4 MHz (51

Table 1 Optical properties of the phantoms for the three different wavelengths of the laser diodes determined by frequency-domain spectroscopy and integrating spheres measurements (mean±standard error).

Wavelength (nm)	678	808	835
Volume filling fraction absorber (%)	Absorption coefficient (mm^{-1})		
0.000	0.027±0.002	0.030±0.004	0.038±0.003
0.656	0.056±0.004	0.102±0.004	0.080±0.002
1.303	0.072±0.003	0.158±0.009	0.109±0.006
1.942	0.101±0.005	0.219±0.010	0.130±0.004
2.572	0.107±0.006	0.255±0.014	0.167±0.019
3.195	0.134±0.016	0.289±0.009	0.193±0.024
Volume filling fraction scatterer (%)	Reduced scattering coefficient (mm^{-1})		
3.0	1.03 ±0.10	0.71 ±0.06	0.71 ±0.06

data points) and a spectral bandwidth of 3.7 kHz. Phase and intensity data were averaged 16 times. The multiplexer and the network analyzer were controlled by a personal computer that was also used to record the measured data. The acquisition time for a single frequency sweep was approximately 400 ms.

3.2 *Scattering and Absorbing Phantoms*

Tissue phantoms were designed to perform an evaluation of the new technique. Several recipes have been published to manufacture solid phantoms with defined scattering and absorption properties.[34] We embedded TiO_2 particles (TiPure 960, DuPont, Mechelen, Belgium) into clear polyester resin (Norpol 340-500, Reichhold, Hamburg, Germany) as described in Ref. 35. A stock solution of 800 mg TiO_2 in 20 ml ethanol was used. The effective diameter of the TiO_2 particles was 350 nm. In order to determine the volume filling fraction of the scatterers (f_{sca}), we performed integrating-sphere measurements[21] for a series of thin phantoms with various amounts of TiO_2 particles. We found that a volume filling fraction of $f_{sca}=3\%$ of the stock solution resulting in reduced scattering coefficients of 1.03 mm^{-1} at 678 nm, 0.71 mm^{-1} at 808 nm, and 0.71 mm^{-1} at 835 nm, respectively (see Table 1), was best suited to mimic the scattering properties of neonatal skin (~1 mm^{-1} in the NIR-wavelength range[24]).

The absorption properties of the phantoms were adjusted with regard to the absorption coefficients of human skin at the wavelengths of interest. The respective data have been calculated using Eq. (8) (see below) from the known extinction spectra of Hb and HbO_2 (Ref. 3) for a total hemoglobin content of 190 g/l, which is typical for fetal blood.[36] The volume fraction occupied by blood vessels was assumed to be 5%.[37] The resulting absorption coefficients at the wavelengths of interest are shown in Fig. 2. They were found to be between 0.01 and 0.1 mm^{-1}. A series of nonscattering phantoms that consisted of various amounts of an absorbing stock solution (1 mg of an infrared dye, ProJet 900 NP by Zeneca Colors, Manchester, England, solved in 10 ml ethanol) in resin was manufactured. The relative absorptivity $\Delta\mu_a/\Delta f_{abs}$ (i.e., the absorption coefficient per unit volume of absorber) of these phantoms was then determined with a conventional absorption spectrometer (Lambda 19, Perkin Elmer, Shelton, Connecticut). It was found that volume filling fractions of the absorber between 0.0 and 3.1% simulated best the various oxygenation states of fetal skin. According to these results, six solid scattering and absorbing phantoms (dimensions: diameter 50 mm, thickness 30 mm) with volume filling fractions of 3% scatterer and 0.0 to 3.1% absorber were manufactured and were used for further investigations.

As can be seen from Eq. (4), the refractive index has to be known in order to deduce the absorption coefficient of the sample. Because more than 93% of the phantom volume is filled with resin, it was assumed that the latter determines the refractive index of the samples. To characterize the phantoms completely, we determined the refractive index of the resin by goniometric reflection measurements. Therefore, a clear resin

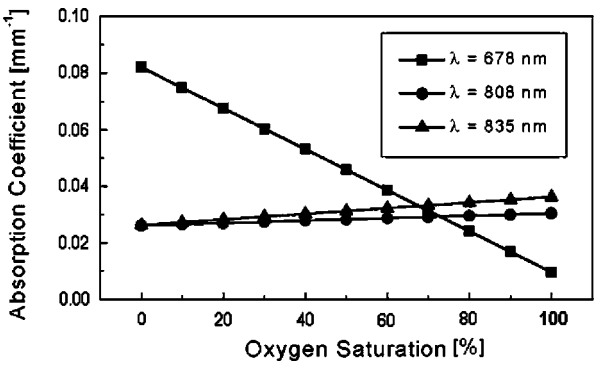

Fig. 2 Calculated absorption coefficients of fetal skin containing 5% of blood as a function of the oxygen saturation.

sample was irradiated using p-polarized light in the wavelength range from 400 to 860 nm. The angle of incidence ϑ of the collimated beam was varied between 15 and 75 deg in steps of 2.5 deg. The refractive index n was obtained by fitting the experimental data to the Fresnel function for p-polarized light $R_p(\vartheta)$:

$$R_p(\vartheta)=\left[\frac{(\sqrt{n^2-\sin^2\vartheta}-\cos\vartheta)^2}{n^2-1}\right]^2. \quad (6)$$

Frequency-domain measurements of the phantoms were performed at source-detector separations between $\rho=3$ mm and $\rho=9$ mm using a single source fiber and a single detector fiber. Equation (4) was then used to derive the absorption coefficient from the measured DC intensity and mean time of flight.

3.3 *Interaction Volume*

Prior to the *in vivo* testing, the interaction volume of the detected photons in the skin was determined using Monte-Carlo simulations as described previously.[38] This volume is of great importance because the measured absorption coefficient represents an average value over the probed sample volume.[39]

Human skin consists of three layers[25,40,41] with different optical properties. The uppermost layer (epidermis) is typically 60 μm thick and does not contain blood vessels. The second layer (dermis) is typically 2 mm thick and contains a fine capillary network of arteries and veins. Underneath the dermis, there is a layer of subcutaneous fat with a thickness of several millimeters, depending on the exact location at the body surface. The optical properties of the epidermis, the dermis, and the subcutaneous fat have been well characterized by several authors.[24–30] In the epidermis, the dominant absorbing chromophore is melanin. The fraction of melanin present in the epidermis f_{mel} depends on the skin type and is reported to vary between 1.3 to 6.3% for lightly pigmented skin and 18 to 43% for heavily pigmented skin.[26] Thus, the absorption coefficient of the epidermis can be calculated from the melanin content (f_{mel}) and the background absorption of unpigmented skin [$\mu_a^{\mathrm{unpigm}}(\lambda)$][25]:

$$\mu_a^{\mathrm{epidermis}}(\lambda)=f_{\mathrm{mel}}\mu_a^{\mathrm{mel}}(\lambda)+(1-f_{\mathrm{mel}})\mu_a^{\mathrm{unpigm}}(\lambda). \quad (7)$$

Here, $\mu_a^{\mathrm{mel}}(\lambda)$ denotes the absorption coefficient of melanin at the wavelength of interest. The absorption spectra of melanin and unpigmented skin can be obtained from the literature.[25] The absorption coefficient of the dermis can be described by the absorption coefficient of unpigmented skin and the absorption coefficient of blood that depends on the concentrations of hemoglobin ([Hb]) and oxyhemoglobin ([HbO_2]):

$$\mu_a^{\mathrm{dermis}}(\lambda)=\mu_a^{\mathrm{unpigm}}(\lambda)+\ln 10\cdot(\epsilon_{\mathrm{HbO_2}}(\lambda)[\mathrm{HbO_2}]+\epsilon_{\mathrm{Hb}}(\lambda)[\mathrm{Hb}]). \quad (8)$$

Here, ϵ_{HbO2} and ϵ_{HB} denote the molar extinction coefficients of HbO_2 and Hb, respectively. The factor ln 10 accounts for the fact that the extinction coefficient is defined as the $\log_{10}$ in contrast to the absorption coefficient. Thus, the various layers contribute differently to the measured absorption coefficient. The epidermal layer can be treated as a background signal, whereas the spectral information about the concentrations of Hb and HbO_2 is contained on the dermal layer.

Table 2 Optical properties of the epidermis (at different melanin contents), the dermis, and the subcutaneous fat for the wavelength of 808 nm. For the dermis, the S[O_2] is 90% and the THC is 116 μmol/l according to a blood volume filling fraction of 5%. The anisotropy factor is assumed to be 0.9 for all layers.[25–28]

	μ_a (mm^{-1})	μ_s (mm^{-1})
Epidermis ($f_{\mathrm{mel}}=0\%$)	0.029	13.4
Epidermis ($f_{\mathrm{mel}}=5\%$)	0.71	13.4
Epidermis ($f_{\mathrm{mel}}=10\%$)	1.40	13.4
Epidermis ($f_{\mathrm{mel}}=15\%$)	2.08	13.4
Epidermis ($f_{\mathrm{mel}}=20\%$)	2.77	13.4
Dermis (S[O_2]=90%, THC=116 μmol/l)	0.046	13.4
Subcutaneous fat	0.0084	11.3

In our simulations, we modeled the skin as a medium consisting of the three layers mentioned above. The thickness of the layers was set to 60 μm for the epidermis and to 2 mm for the dermis. A typical value for the depth of the subcutaneous fat layer is 8 mm. The influence of the underlying tissue layers can be neglected, provided that the detected photons do not penetrate more than 1 cm into the tissue for the considered source-detector separations. Thus, the thickness of the subcutaneous fat layer can be set to infinity in the Monte-Carlo model.

The absorption coefficients of the epidermis and dermis were calculated from Eq. (7) and Eq. (8). A volume filling fraction of blood of 5% according to a THC of 116 μmol/l and an oxygen saturation of 90% was assumed for the dermis. Four series of simulations were performed where the melanin content of the epidermis was varied ($f_{\mathrm{mel}}=5$, 10, 15 and 20%). The reduced scattering coefficients of the dermis and epidermis were calculated as described in Ref. 25. The absorption coefficient and the reduced scattering coefficient of subcutaneous fat were obtained from Ref. 28. The scattering coefficients of the skin layers were calculated from the reduced scattering coefficients assuming the anisotropy factor of 0.9 (Ref. 30). For refractive indices of the various skin layers, a value of $n=1.4$ was used.[42] The resulting optical properties for a wavelength of 808 nm are shown in Table 2.

In the calculations, photons were launched into the multilayered semi-infinite medium. The illuminated area and the angular distribution of the launched and detected photons were chosen according to the diameter (600 μm) and numerical aperture (0.2) of the employed source and detector fiber. The propagation of the photons in the medium was calculated using a variable step size Monte-Carlo algorithm that was described in Ref. 38. When a photon crossed the boundary between two layers, the new position of the photon was calculated according to the optical properties of the new layer.[39] In addition, the Fresnel reflections at the surface of the skin were taken into account.

On the surface of the medium, nine detector fibers were defined at distances between 2 and 10 mm from the source fiber in steps of 1 mm. For those photons that were diffusely reflected, the positions and the angles at which the photons left the surface were calculated. From these data the probability for launched photons to be detected by one of the detector fibers could be determined. The simulation was terminated when a total number of 1000 photons was detected at the largest distance (10 mm) from the source fiber. Consequently, much larger numbers of photons were registered for the smaller distances (>30,000 for the smallest distance of 2 mm).

For further data processing, the trajectories of those photons that reached one of the detector fibers were stored in the computer. Therefore, a Cartesian coordinate system was defined such that the surface of the medium was located in the x-y plane and the z-axis is perpendicular to the surface. The (x,y,z) coordinates of the source and detector fiber were (0,0,0) and $(\rho,0,0)$, respectively. For those photons that entered the detector fiber located at $x=\rho$, a grid of cubic voxels was defined where the basic length was set to $\Delta l_\rho = \rho/100$. In this discrete space, the position of a single voxel could be characterized by three integer numbers i, j and k, where the coordinates of the voxel were $(x_i, y_j, z_k) = (i*\Delta l_\rho, j*\Delta l_\rho, k*\Delta l_\rho)$. As a measure of the interaction volume, we defined the interaction density of the detected photons $S_\rho(x_i, y_j, z_k)$ as the number of scattering events of the detected photons in the voxel located at the position (x_i, y_j, z_k). A two-dimensional projection $S_\rho(x_i, z_k)$ of the interaction volume can be obtained by adding the values of the interaction density at fixed x_i and z_k positions for all y_j positions:

$$S_\rho(x_i, z_k) = \sum_j S_\rho(x_i, y_j, z_k). \tag{9}$$

In reflection geometry, this interaction volume has the shape of a banana and is therefore often referred to as the ''photon-banana.'' As a measure of the mean penetration depth ($\langle z \rangle$) the center of mass of the interaction density at half of the distance between the source and detector fiber $\rho/2$ was calculated:

$$\langle z \rangle = \frac{\Sigma_k z_k \cdot S_\rho(\rho/2, z_k)}{\Sigma_k S_\rho(\rho/2, z_k)}. \tag{10}$$

Additionally, the mean path length of the photons in the individual layers can easily be obtained from the stored photon trajectories.

3.4 *In vivo Measurements*

In contrast to the existing ''large-volume'' methods for the measurement of the oxygen saturation and total hemoglobin content *in vivo*,[10–12] the small-volume approach measures the average absorption properties of the epidermis and dermis weighted by the interaction density of the two layers. To interpret the measured *in vivo* data, we consider a turbid medium that consists of two layers A and B with different scattering coefficients (μ_s^A and μ_s^B) and absorption coefficients (μ_a^A and μ_a^B) as shown in Fig. 3. The photons that are scattered into the detector fiber travel different paths in the medium. In Fig. 3, the trajectory of a single photon between the source and the detector fiber is shown. The length of the trajectory in layers A and B is referred to as d^A and d^B, respectively. For a large number of photons that are scattered into the detector fiber, the average pathlengths of the photons in layers A and B are denoted $\langle d^A \rangle$ and $\langle d^B \rangle$. When the multilayered medium in Fig. 3 is examined using the MBL [Eq. (4)], the average absorption coefficient μ_a of the two layers A and B will be obtained whereby the average is weighted with the average pathlengths of the photons in the medium:

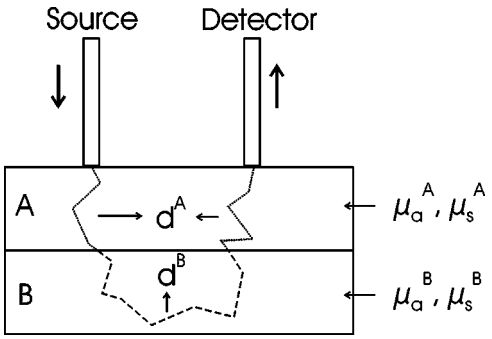

Fig. 3 Schematic drawing of the trajectory of a single photon between a source and a detector fiber in a turbid medium, which consists of two layers A and B with different optical properties (scattering coefficients μ_s^A and μ_s^B, absorption coefficients μ_a^A and μ_a^B). The pathlengths of the photon in layers A and B are d^A and d^B, respectively. When a large number of photons with different trajectories between source and detector fibers is considered, the mean pathlengths $\langle d^A \rangle$ and $\langle d^B \rangle$ are relevant.

$$\mu_a = \frac{\langle d^A \rangle \mu_a^A + \langle d^B \rangle \mu_a^B}{\langle d^A \rangle + \langle d^B \rangle} = f^A \cdot \mu_a^A + (1 - f^A) \cdot \mu_a^B. \tag{11}$$

Here, $f^A = \langle d^A \rangle / (\langle d^A \rangle + \langle d^B \rangle)$ denotes the fractional contribution of the average pathlength of the photons in the upper layer A. Regarding the measurement of the absorption coefficient μ_a of human skin using the modifiend MBL, Eq. (11) can be written as:

$$\mu_a(\lambda) = f^{\text{epidermis}} \mu_a^{\text{epidermis}}(\lambda) + (1 - f^{\text{epidermis}}) \mu_a^{\text{dermis}}(\lambda), \tag{12}$$

where $f^{\text{epidermis}}$ denotes the fractional contribution of the epidermis to the absorption coefficient. The absorption coefficient of the epidermis $\mu_a^{\text{epidermis}}$ follows from Eq. (7). The absorption coefficient of the dermis μ_a^{dermis} depends on the concentrations of Hb and HbO_2 as described in Eq. (8). In order to derive the hemoglobin concentration in the tissue, the absorption coefficient μ_a is measured at two different wavelengths. The concentrations of Hb and HbO_2 can be calculated using Eqs. (7), (8), and (12) provided that the fractional contribution of absorption and the melanin content of the epidermis are known. The oxygen saturation and the total hemoglobin content finally follow from:

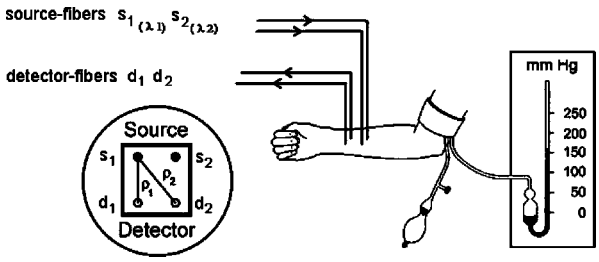

Fig. 4 *In vivo* experiment to determine the oxygen saturation and the total hemoglobin content at the forearm of a volunteer using a blood pressure cuff to occlude the arm vessels. The inset shows the arrangement of the source and detector fibers [wavelengths: $\lambda_1 = 678$ nm, $\lambda_2 = 808$ nm; source-detector separations for λ_1: $\rho_1 = 5$ mm, $\rho_2 = 7$ mm; source-detector separations for λ_2 in analogy (not depicted)].

$$S[O_2] = \frac{[HbO_2]}{[Hb]+[HbO_2]} \times 100\%$$

and

$$THC = [Hb]+[HbO_2]. \quad (13)$$

In this study, *in vivo* measurements were performed on the forearm of a healthy Caucasian volunteer with light-colored skin. According to Ref. 26, the value of $f_{mel} = 5\%$ was used for the evaluation of the measured absorption coefficients. The fractional contribution of the epidermal layer to the overall absorption coefficient was estimated from the Monte-Carlo simulations.

In order to demonstrate the feasibility of the new technique to determine $S[O_2]$ and THC *in vivo*, a homemade applicator consisting of two source and two detector fibers was positioned on the forearm of the volunteer at rest (blood pressure at rest was 115/80 mm Hg). The arrangement of the fibers is presented in Fig. 4. The dimensions of the applicator head are $10 \times 8 \times 10$ mm^3 (length×width×height). A homemade fiber switch consisting of a magnetic shutter and a 2-in-1 fiber coupler allowed consecutive recording of the signal obtained by the two detector fibers. For the *in vivo* measurements, two wavelengths ($\lambda_1 = 678$ nm, $\lambda_2 = 808$ nm) were chosen. At 678 nm, the difference of the absorption coefficients of oxy- and deoxyhemoglobin is maximal while at 808 nm there is an isosbestic point of the two absorbers (see Fig. 2).[3] Thus, the sensitivity to detect small changes in $S[O_2]$ can be expected to be largest for the available wavelengths. For both wavelengths, the refractive index of $n = 1.4$ was assumed.[42]

At the beginning of the *in vivo* measurements, baseline data were acquired over 5 minutes. Thereafter, a pneumatic blood pressure cuff was inflated to a pressure of 150 to 160 mm Hg for 4.5 minutes inducing vascular occlusion. After release of the cuff, measurements of the absorption coefficients were continued for another 5 minutes. The acquisition time for a single data set was approximately 15 seconds. During the experiment, the data sets were collected in intervals of 30 seconds. The personal computer used to control the experimental setup was also employed to calculate $S[O_2]$ and THC from the measured quantities. The sequence of the steps that were performed for the calculation of the oxygen saturation and the total hemoglobin content from the frequency-domain data is outlined in Fig. 5.

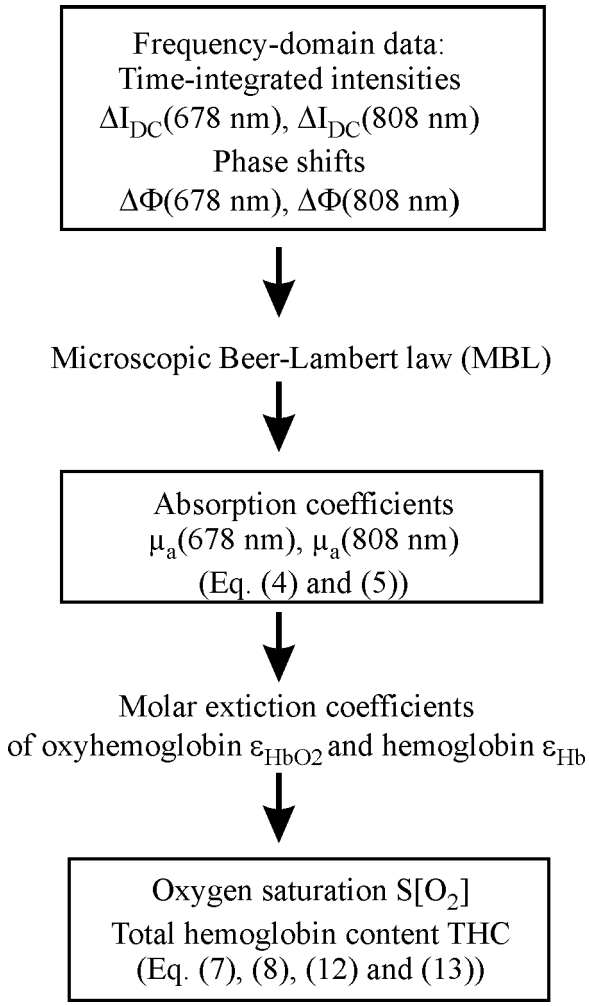

Fig. 5 Sequence of the determination of the oxygen saturation $S[O_2]$ and the total hemoglobin content THC from the frequency-domain data.

4 Results

4.1 *Phantom Measurements*

4.1.1 *Refractive index*

The refractive index of the phantoms was determined from the goniometric reflection measurements using Eq. (6) as described above. The result of these measurements is shown in Fig. 6. From the measured values of the refractive index, the following two-parameter Sellmeier formula was obtained:

$$n^2(\lambda) = 1 + \frac{1.3025\{\lambda\}^2}{\{\lambda\}^2 - (0.1375)^2} \quad (\{\lambda\} \text{in } \mu\text{m}). \quad (14)$$

The refractive index of the phantoms was calculated at the wavelengths of interest using Eq. (14).

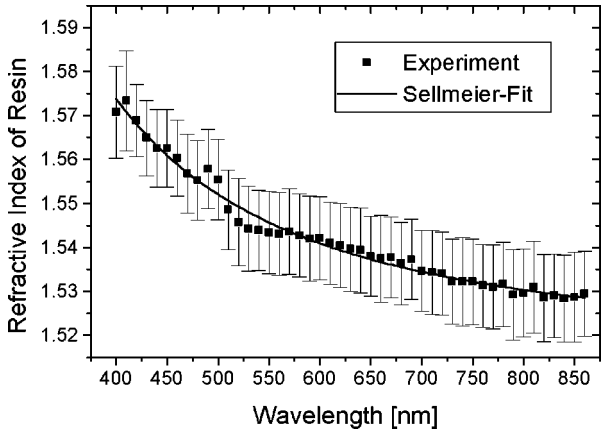

Fig. 6 Refractive index of resin: experimental values (symbols, mean and standard error) and Sellmeier fit according to Eq. (14) (solid line).

4.1.2 *Absorption properties*

Frequency-domain measurements were then performed for the six phantoms containing different amounts of absorber to determine the time-integrated intensity I_{DC} and the mean time of flight $\langle t \rangle$ of the detected photons. Figure 7 shows the time-integrated intensity I_{DC} as a function of the mean time of flight $\langle t \rangle$ at various source-detector separations between 3 and 9 mm for the wavelength of $\lambda = 678$ nm. The mean time of flight varied between 150 and 550 ps corresponding to a mean pathlength of the photons $\langle L \rangle = c_n \langle t \rangle$ between 29 and 107 mm. Thus, it exceeded the source-detector separation by a factor of up to 12. As predicted by the modified MBL, the logarithm of the DC intensity decreased linearly with increasing time of flight. The correlation coefficients for all wavelengths were greater than 0.98. According to Eq. (4), the absorption coefficient of the sample can be obtained from the slope of the $\ln\{I_{DC}\}$ vs. $\langle t \rangle$ plots. The resulting absorption coefficients are presented in Fig. 8 for all employed wavelengths. A linear dependence of μ_a from the volume filling fraction of the absorbers was obtained (correlation coefficient

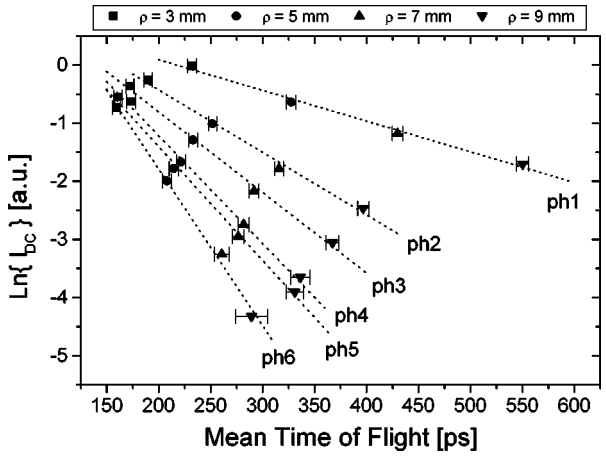

Fig. 7 Logarithm of the time-integrated intensity as a function of the mean time of flight for the various phantoms at a wavelength of λ=678 nm (symbols, mean and standard error; dotted line, linear regression). All correlation coefficients are >0.98.

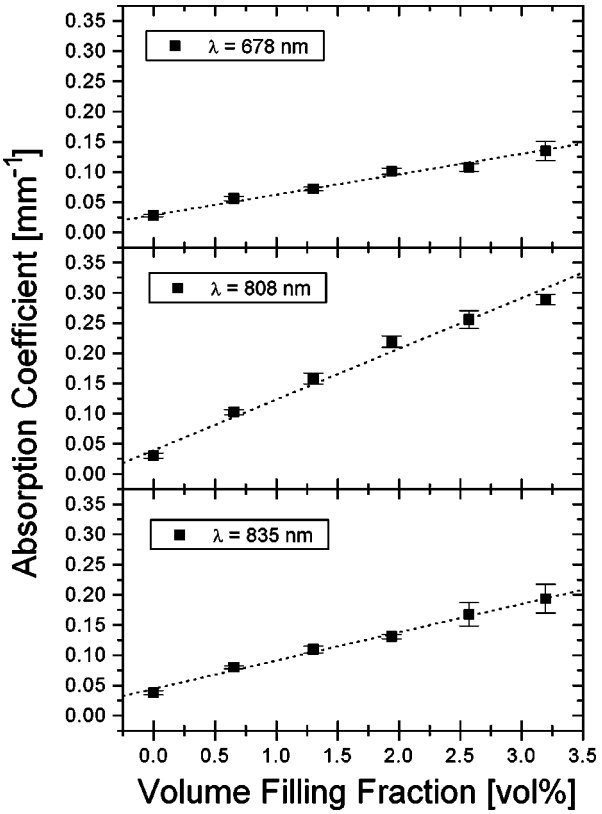

Fig. 8 Absorption coefficient of the phantoms as a function of the volume filling fraction of the absorber (symbols, mean and standard error; dotted line, linear regression). The regression coefficients are $R = 0.9929$ (λ=678 nm), $R = 0.9917$ (λ=808 nm), and $R = 0.9885$ (λ = 835 nm).

$R = 0.993$ for λ=678 nm, 0.992 for λ=808 nm, and 0.989 for λ=835 nm). The relative absorptivities $\Delta\mu_a / \Delta f_{abs}$ obtained from the slopes of Fig. 8 were compared to the relative absorptivities of the non-scattering phantom samples determined using the conventional absorption spectrometer. As can be seen in Fig. 9, the frequency-domain technique data agreed very well with the results obtained from the conventional spectrophotometer. The resulting optical properties of the phantoms used in this study are summarized in Table 1.

4.2 *Monte-Carlo Simulations*

Figure 10 shows a typical result for the interaction density as a function of the depth in the turbid medium at a distance of ρ=5 mm from the source fiber. The optical properties correspond to the wavelength of 808 nm and the melanin content in the dermis of 5% (Table 2). The banana-like shape of the probed sample volume is clearly visible. The mean penetration depth $\langle z \rangle$ is shown in Fig. 11 as a function of ρ for the wavelength of 808 nm. As can be seen in this figure, $\langle z \rangle$ increases linearly with ρ from 1.2 mm at ρ=2 mm to approximately 5 mm at ρ=10 mm. No significant dependence of the mean penetration depth on the melanin content of the epidermis was found in the Monte-Carlo simulations between ρ=2 and 9 mm.

Furthermore, the ratio of the pathlength of the photons in the epidermis to the total pathlength $f^{epidermis}$ was calculated

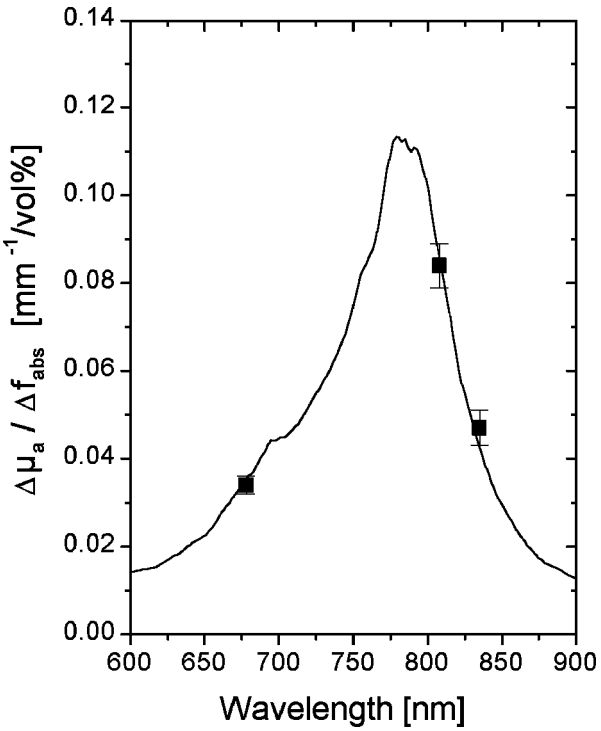

Fig. 9 Comparison of the relative absorptivities measured using the frequency-domain spectrometer (symbols, mean and standard error) with the mean relative absorptivity determined with a conventional absorption spectrometer for a series of non-scattering phantoms (solid line).

for the different values of f_{mel}. The dependence of $f^{\mathrm{epidermis}}$ on the source-detector separation is shown in Fig. 12 for the wavelength of 808 nm. For the source-detector separation of 2 mm and the melanin content of $f_{\mathrm{mel}}=5\%$, about 2.7% of the

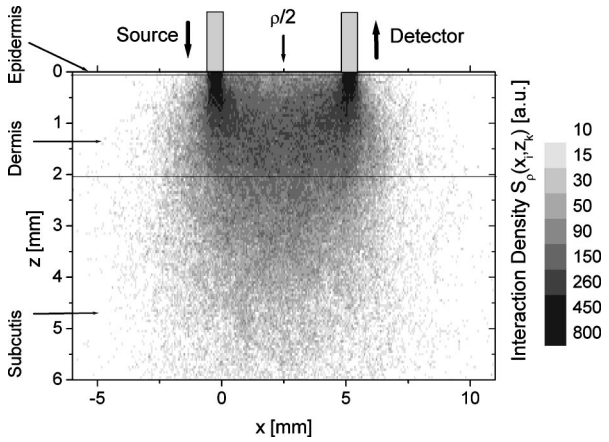

Fig. 10 Interaction density $S_\rho(x_i, z_k)$ of the detected photons for a three-layer semi-infinite model of human skin (epidermis, dermis, and subcutis) determined with a Monte-Carlo simulation for a source-detector separation of ρ=5 mm (logarithmic grayscale, arbitrary units). The layer boundaries are at $z=0.06$ mm and $z=2.06$ mm. The optical properties of the layers correspond to the epidermis, dermis, and subcutaneous fat at the wavelength of 808 nm and the melanin content of 5% in the epidermis. Source and detector fiber are located at $x=0$ mm and $x=5$ mm, respectively.

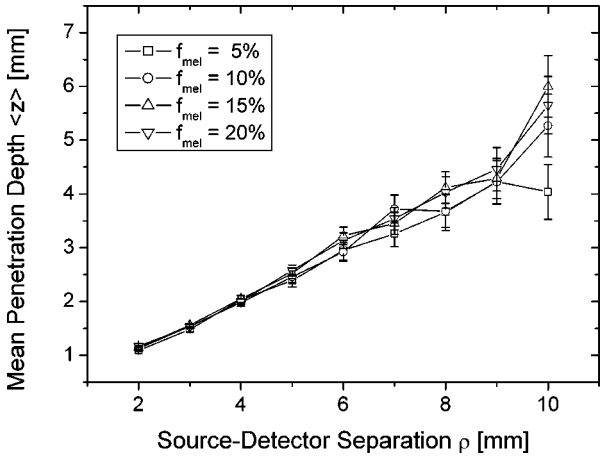

Fig. 11 Penetration depths of the detected photons as a function of the source-detector separation determined with a Monte-Carlo simulation in a three-layer semi-infinite medium for different melanin contents f_{mel} in the epidermis (mean±standard error). The optical properties correspond to the wavelength of 808 nm. For the small source-detector separations, a larger number of photons was detected. Thus, a better statistical accuracy was achieved.

interaction events occurred within the first layer of the medium. The fraction decreases to approximately 1.1% at ρ=5 mm and 0.8% at ρ=7 mm. At the wavelength of 678 nm and the melanin content of 5%, the value of 0.9% at ρ=5 and 0.7% at ρ=7 mm was obtained for $f^{\mathrm{epidermis}}$. With regard to these findings, a mean value of $f^{\mathrm{epidermis}}=0.9\%$ was used for the processing of the *in vivo* data.

4.3 *In vivo Measurements*

Figure 13 shows the absorption coefficients at 678 and 808 nm and the calculated concentrations of Hb and HbO_2 in the probed region before, during, and after occlusion of the blood vessels. Using Eqs. (12) and (13), the total hemoglobin content and the oxygen saturation have been calculated from the

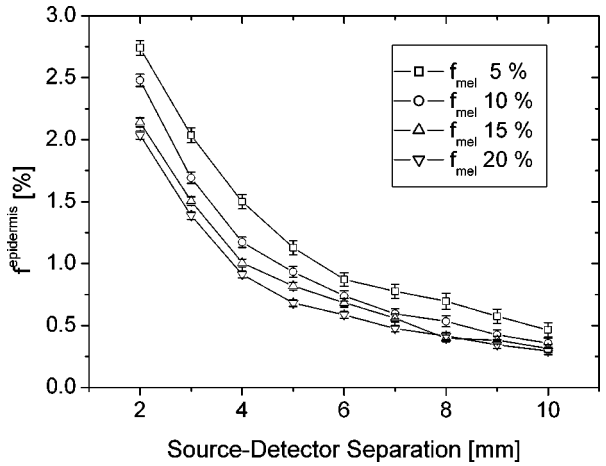

Fig. 12 Fractional contribution $f^{\mathrm{epidermis}}$ of the epidermal layer (thickness 60 μm[26]) to the photon pathlength in human skin determined from Monte-Carlo simulations at the wavelength of 808 nm for different source-detector separations and different melanin contents f_{mel} (mean±standard error).

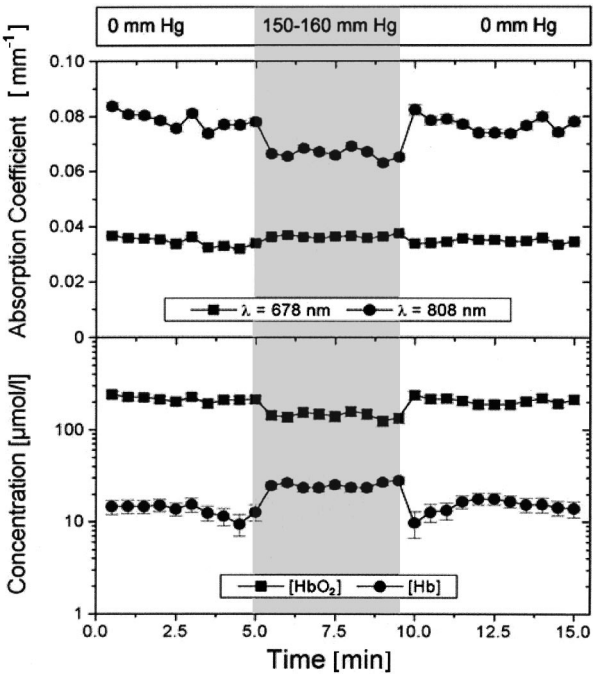

Fig. 13 Absorption coefficient and concentration of hemoglobin and oxyhemoglobin determined in the *in vivo* experiment. The error bars represent the uncertainties due to experimental errors. The shaded area indicates the period of cuff occlusion.

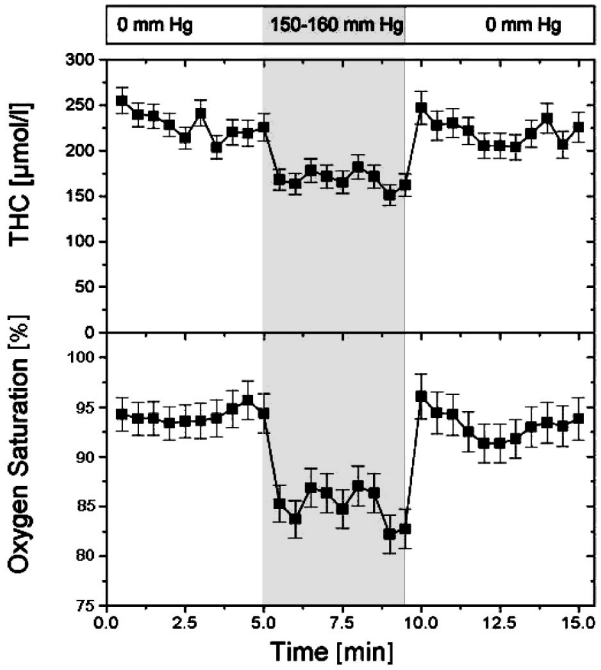

Fig. 14 Result of the *in vivo* determination of the oxygen saturation and the total hemoglobin content. The error bars represent the uncertainties due to experimental errors. The shaded area indicates the period of cuff occlusion.

measured data assuming a fractional melanin content of $f_{\mathrm{mel}} = 5\%$ and an average fractional pathlength in the epidermis of $f^{\mathrm{epidermis}} = 0.9\%$. The result of these calculations is shown in Fig. 14. During occlusion, the calculated THC rapidly decreased from approximately 220 to 250 μmol/l to values between 150 and 190 μmol/l and the calculated $S[O_2]$ dropped from approximately 94 to 95% to 82 to 86%. After release of the blood pressure cuff, THC and $S[O_2]$ increased rapidly and returned to the values measured before occlusion of the blood vessels.

5 Discussion

The modified time-integrated MBL has earlier been demonstrated to allow the determination of absorption coefficients in turbid media with optical properties comparable to those of biological tissues at small source-detector separations (between 3 and 10 mm).[21] In this study, we evaluated its applicability towards the monitoring of the oxygen saturation and total hemoglobin content of fetal skin to provide minimally invasive oximetry *sub partu*.

First, a total of six scattering and absorbing phantoms with optical properties comparable to those of neonate skin in the red and near-infrared spectral range were manufactured as described in Ref. 35. These phantoms consisted of a clear transparent polyester matrix and TiO_2 particles with a volume filling fraction of 3% as scatterers. The phantoms contained various amounts of an infrared dye ranging from 0.0 to 3.1% to simulate various oxygenation states of blood in fetal skin tissue.[24,30] As predicted by the modified MBL [Eq. (4)], we obtained excellent linear correlations between the logarithm of the time-integrated intensity and the mean time of flight at all investigated wavelengths ($R > 0.98$, Fig. 7). The relative absorptivities obtained from the slopes of the absorption coefficients as a function of the volume filling fractions of absorbers (Fig. 8) were compared to the relative absorptivity spectrum obtained in a non-scattering sample using a conventional absorption spectrometer (''gold standard''). The agreement between the two methods was again excellent as can be seen in Fig. 9. This indicates that the modified MBL is well suited for the determination of the absorption coefficient of human neonate skin at the considered source-detector separations between 3 and 9 mm.

In contrast to the optically homogeneous phantoms, human skin consists of various layers with varying optical properties. In such inhomogeneous tissues, the contribution of each layer within the probed sample volume to the measured absorption coefficient has to be known in order to interpret the measured data correctly. Especially the knowledge of the background absorption coefficient (defined as all contributions to μ_a that are not due to hemoglobin absorption) is a prerequisite to accurately derive $S[O_2]$ and THC from the measured quantities.[12] Absorption in the uppermost epidermal layer is mainly due the chromophore melanin. Its fractional content in the epidermis depends on the skin type.[26] In standard pulse oximetry, strong melanin absorption has led to misleading results. In Afro-Caribbean fetuses, for example, it contributes significantly as a background signal to the measured extinction coefficients that ultimately determine $S[O_2]$.[9]

We investigated the influence of the layered skin structure and the contributions from absorption in the individual layers to the measured absorption coefficient using the Monte-Carlo method.[38] The optical properties of the tissue layers were obtained from the literature.[24–30] The background absorption co-

efficients of both layers have been calculated using published data for the absorption coefficients of melanin and unpigmented skin.[25] The melanin content in the epidermal layer was varied to simulate different skin types from light to dark colored. The Monte-Carlo simulations showed that the mean penetration depth increases linearly with the separation between the source and detector fiber from approximately 1.2 mm (ρ=2 mm) to 5 mm (ρ=10 mm, Fig. 11). Thus, this technique is definitely capable to detect the oxygen saturation in the dermis at the source-detector separations used here. As can be seen in Fig. 11, no significant dependence of the mean penetration depth from the melanin content of the epidermis can be observed for the employed source-detector separations of 5 and 7 mm. For these source-detector separations, the average value of $f^{\text{epidermis}}=0.9\%$ was found for the fractional contribution of the epidermis to the overall absorption coefficient at the considered wavelengths (Fig. 12). Thus, epidermal absorption can be neglected in Eq. (12), if $\mu_a^{\text{epidermis}}(\lambda)$ is smaller than or comparable to $\mu_a^{\text{dermis}}(\lambda)$, i.e., for completely unpigmented skin ($f_{\text{mel}}=0\%$). Under practical conditions, however, the epidermal absorption at 808 nm exceeds the absorption coefficient in the dermis even for light-colored skin ($f_{\text{mel}}=5\%$) by a factor of 18 and up to approximately 70 for dark-colored skin ($f_{\text{mel}}=20\%$) (Table 2). In this case, a neglect of the epidermal background contribution would lead to significant deviations of the calculated values for $S[O_2]$ and THC, because the contributions from both skin layers become comparable [i.e., $f^{\text{epidermis}}\mu_a^{\text{epidermis}}\approx(1-f^{\text{epidermis}})\mu_a^{\text{dermis}}$ in Eq. (12)]. It should also be mentioned that the weighting factor $f^{\text{epidermis}}$ depends on the thickness of the epidermis. The thickness was assumed to be 60 μm in the Monte-Carlo simulations, but it can vary *in vivo*. Nevertheless, by using Eq. (12) in combination with literature data for the melanin content of the epidermis,[26] the new method is in principle able to account for the contribution of the epidermis to the absorption coefficient of the skin caused by melanin. Thus, this technique might in the future overcome the limitation of standard pulse oximeters, which do not allow a reliable quantification of the oxygen saturation in the skin of Afro-Carribean fetuses.[9]

Finally, an *in vivo* feasibility test was performed using the forearm of a healthy Caucasian volunteer with light-colored skin. We obtained baseline values for the tissue oxygenation of 94 to 95% using source-detector separations of 5 and 7 mm. These baseline values are slightly lower than the value for the oxygen saturation of pure arterial blood, which is commonly reported to be 97% in healthy adults.[36] This finding may indicate that mainly arterial capillaries are located in the volume that is probed in this experiment. After occlusion of the upper arm with a blood pressure cuff, the measured oxygen saturation decreased to 80 to 86%. These values are close to the reported values of pure venous blood.[36]

The baseline values of THC were between 200 and 260 μmol/l. The total hemoglobin content decreased to 150 to 180 μmol/l after occlusion of the upper arm indicating a vasocontraction of the dermal blood vessels. After release of the blood pressure cuff, $S[O_2]$ and THC returned to their initial baseline values. Thus, these results show that the new technique is applicable in patient. The calculated data were close to the values to be expected for healthy human subjects.

Another important aspect for the practical application of the proposed method is the temporal resolution. The total acquisition time for a single $S[O_2]$ and THC data point in our setup is approximately 15 seconds. The time is limited by the consecutive readout of the two measurement channels using the magnetic fiber switch. By using an additional APD for the second detector fiber, the temporal resolution can easily be reduced to a few seconds. On the other hand, a temporal resolution of 15 seconds can be considered satisfactory compared to the time intervals required to collect fetal blood samples in clinical practice.

Further work will be directed towards a systematic clinical evaluation including the comparison to blood gas analyzers representing the golden standard of clinical medicine.

6 Conclusions

In conclusion, we have demonstrated that the modified time-integrated microscopic Beer-Lambert law can be used to absolutely determine the absorption coefficient of tissue phantoms with optical properties similar to those of human neonate skin with varying oxygen saturations at source-detector separations smaller than 10 mm. Using the described technique, we were able to determine $S[O_2]$ and THC *in vivo* with a temporal resolution of approximately 15 seconds. The proposed method is able to quantitatively account for variations in the background absorption due to different amounts of melanin present in the epidermal skin layer. The technique is well suited for minimally invasive oxygen monitoring where small applicator dimensions and short acquisition time are required (e.g., fetal oxygen monitoring *sub partu*). The method, however, is still subject to clinical evaluation.

Acknowledgments

This work was supported by the Ministerium für Bildung, Wissenschaft, Forschung und Technologie (BMBF, Germany) grant No. 13N7067/2.

References

1. G. A. Millikan, ''Oximeter, instrument for measuring continuously oxygen saturation of arterial blood in man,'' *Rev. Sci. Instrum.* **13**, 434 (1942).
2. I. Yoshiya, Y. Shimada, and K. Tanaka, ''Spectrophotometric monitoring of arterial oxygen saturation in the fingertip,'' *Med. Biol. Eng.* **18**, 27–32 (1980).
3. S. A. Prahl, ''Optical absorption of hemoglobin,'' http://ee.ogi.edu/omlc/spectra/hemoglobin/index.html (1999).
4. A. O. Soubani, ''Noninvasive monitoring of oxygen and carbon dioxide,'' *Am. J. Emerg. Med.* **19**, 141–146 (2001).
5. P. M. Middleton and J. A. Henry, ''Pulse oxymetry: evolution and directions,'' *Int. J. Clin. Pract.* **54**, 438–444 (2000).
6. J. E. Sinex, ''Pulse oximetry: principles and limitations,'' *Am. J. Emerg. Med.* **17**, 59–67 (1999).
7. V. König, R. Huch, and A. Huch, ''Wie kann ein Pulsoxymeter kalibriert werden?'' in *Hypoxische Gefährdung des Fetus sub partu—Klinik und neue Überwachungsverfahren*, R. Knitza, Ed., pp. 111–116, Steinkopf Verlag, Darmstadt, Germany (1994).
8. Y. Mendelson, ''Pulse oximetry: theory and applications for noninvasive monitoring,'' *Clin. Chem.* **38**(9), 1601–1607 (1992).
9. D. D'Antona, C. J. Aldrich, P. O'Brien, S. Lawrence, D. T. Delpy, and J. S. Wyatt, ''Recent advances in fetal near infrared spectroscopy,'' *J. Biomed. Opt.* **2**, 15–21 (1997).
10. S. Fantini, M. A. Franceschini, J. S. Maier, S. A. Walker, B. Barbieri, and E. Gratton, ''Frequency-domain multichannel optical detector for noninvasive tissue spectroscopy and oxyimetry,'' *Opt. Eng.* **34**, 32–42 (1995).

11. M. A. Franceschini, E. Gratton, and S. Fantini, ''Noninvasive optical method of measuring tissue and arterial saturation: an application to absolute pulse oximetry of the brain,'' *Opt. Lett.* **24**, 829–831 (1999).
12. D. M. Hueber, M. A. Franceschini, H. Y. Ma, Q. Zhang, J. R. Ballesteros, S. Fantini, D. Wallace, V. Ntziachristos, and B. Chance, ''Non-invasive and quantitative near-infrared haemoglobin spectrometry in the piglet brain during hypoxic stress, using a frequency-domain multidistance instrument,'' *Phys. Med. Biol.* **46**, 41–62 (2001).
13. B. B. Das, F. Liu, and R. R. Alfano, ''Time-resolved fluorescence and photon migration studies in biomedical and model random media,'' *Rep. Prog. Phys.* **60**, 227–292 (1997).
14. M. S. Patterson, B. Chance, and B. C. Wilson, ''Time resolved reflectance and transmittance for the noninvasive measurement of tissue optical properties,'' *Appl. Opt.* **28**, 2331–2336 (1989).
15. J. R. Lakowicz and K. W. Berndt, ''Frequency-domain measurements of photon migration in tissues,'' *Chem. Phys. Lett.* **166**, 246–252 (1990).
16. S. R. Arridge, M. Cope, and D. T. Delpy, ''The theoretical basis for the determination of optical pathlengths in tissue: temporal and frequency analysis,'' *Phys. Med. Biol.* **37**, 1531–1560 (1992).
17. S. Fantini, M. A. Franceschini, and E. Gratton, ''Semi-infinite-geometry boundary problem for light migration in highly scattering media: a frequency-domain study in the diffusion approximation,'' *J. Opt. Soc. Am. B* **11**, 2128–2138 (1994).
18. K. M. Yoo, F. Liu, and R. R. Alfano, ''When does the diffusion approximation fail to describe photon transport in random media?'' *Phys. Rev. Lett.* **64**, 2647–2650 (1990).
19. I. V. Yaroslavsky, A. N. Yaroslavsky, H. J. Schwarzmaier, G. G. Akchurin, and V. V. Tuchin, ''New approach to Monte Carlo simulation of photon transport in the frequency-domain,'' *Proc. SPIE* **2626**, 45–54 (1995).
20. I. V. Yaroslavsky, A. Terenji, S. Willmann, A. N. Yaroslavsky, H. Busse, and H.-J. Schwarzmaier, ''Small-volume tissue spectroscopy using photon-density waves: apparatus and technique,'' *Proc. SPIE* **3597**, 465–473 (1999).
21. S. Willmann, A. Terenji, J. Osterholz, H.-J. Schwarzmaier, and P. Hering, ''Absolute absorber quantification in turbid media at small source-detector separations,'' *Appl. Phys. B: Lasers Opt.* **54**, 589–595 (2002).
22. Y. Tsuchiya and T. Urakami, ''Photon migration model for turbid biological medium having various shapes,'' *Jpn. J. Appl. Phys.* **34**, 79–81 (1995).
23. Y. Tsuchiya and T. Urakami, ''Quantitation of absorbing substances in turbid media such as human tissue based on the microscopic Beer-Lambert law,'' *Opt. Commun.* **144**, 269–280 (1997).
24. I. S. Saidi, S. L. Jacques, and K. F. Tittel, ''Mie and Rayleigh modeling of visible-light scattering in neonatal skin,'' *Appl. Opt.* **34**, 7410–7418 (1995).
25. S. L. Jacques, ''Skin optics,'' http://omlc.ogi.edu/news/jan98/skinoptics.html (1998).
26. S. L. Jacques and D. J. McAuliffe, ''The melanosome: threshold temperature for explosive vaporization and internal absorption coefficient during pulsed laser irradiation,'' *Photochem. Photobiol.* **53**, 769–775 (1991).
27. M. J. C. Van Gemert, S. L. Jacques, H. J. C. M. Sterenborg, and W. M. Star, ''Skin optics,'' *IEEE Trans. Biomed. Eng.* **36**, 1146–1154 (1989).
28. C. R. Simpson, M. Kohl, M. Essenpreis, and M. Cope, ''Near-infrared optical properties of ex vivo human skin and subcutaneous tissues measured using the Monte Carlo inversion technique,'' *Phys. Med. Biol.* **43**, 2465–2478 (1998).
29. W. F. Cheong, S. A. Prahl, and A. J. Welch, ''A review of the optical properties of biological tissues,'' *IEEE J. Quantum Electron.* **26**(12), 2166–2185 (1990).
30. I. S. Saidi, ''Transcutaneous optical measurement of hyperbilirubinemia in neonates,'' PhD Thesis, Rice University, Houston, Texas (1992).
31. H. Zhang, M. Miwa, Y. Yamashita, and Y. Tsuchiya, ''Quantitation of absorbers in turbid media using time-integrated spectroscopy based on microscopic Beer-Lambert law,'' *Jpn. J. Appl. Phys.* **37**, 2724–2727 (1998).
32. H. Zhang, T. Urakami, Y. Tsuchiya, Z. Lu, and T. Hiruma, ''Time integrated spectroscopy of turbid media based on the microscopic Beer-Lambert law: application to small phantoms having different boundary conditions,'' *J. Biomed. Opt.* **4**, 183–190 (1999).
33. S. J. Madsen, E. R. Anderson, R. C. Haskell, and B. J. Tromberg, ''Portable, high-bandwidth frequency-domain photon migration instrument for tissue spectroscopy,'' *Opt. Lett.* **19**, 1934–1937 (1994).
34. U. Sukowski, F. Schubert, D. Grosenick, and H. Rinneberg, ''Preparation of solid phantoms with defined scattering and absorption properties for optical tomography,'' *Phys. Med. Biol.* **41**, 1823–1844 (1996).
35. S. A. Prahl, ''Optical phantoms,'' http://omlc.ogi.edu/classroom/phantom/index.html (1999).
36. G. Thewes, ''Blood gas transport and acid-base balance,'' in *Human Physiology*, R. F. Schmidt and G. Thews, Eds., pp. 489–507, Springer-Verlag, Berlin, Heidelberg, New York (1983).
37. E. Witzleb, ''Functions of the vascular system,'' in *Human Physiology*, R. F. Schmidt and G. Thewes, Eds., pp. 397–455, Springer-Verlag, Berlin, Heidelberg, New York (1983).
38. S. Willmann, H.-J. Schwarzmaier, A. Terenji, I. V. Yaroslavsky, and P. Hering, ''Quantitative microspectrophotometry in turbid media,'' *Appl. Opt.* **38**, 4904–4913 (1999).
39. M. Hiraoka, M. Firbank, M. Essenpreis, M. Cope, S. R. Arridge, P. Van Der Zee, and D. T. Delpy, ''A Monte Carlo investigation of optical pathlength in inhomogeneous tissue and its application to near-infrared spectroscopy,'' *Phys. Med. Biol.* **38**, 1859–1876 (1993).
40. G. F. Odland, ''Structure of the skin,'' in *Physiology, Biochemistry, and Molecular Biology of the Skin*, 2nd ed., L. A. Goldsmith, Ed., pp. 3–62, Oxford University Press, New York, Oxford (1991).
41. K. S. Stenn, ''The skin,'' in *Cell And Tissue Biology*, 6th ed., L. Weiss, Ed., pp. 539–572, Urban & Schwarzenberg, Baltimore, Munich (1988).
42. A. Roggan, ''Dosimetrie thermischer Laseranwendungen in der Medizin,'' in *Fortschritte in der Lasermedizin*, Vol. 16, G. J. Müller and H. P. Berlien, Eds., p. 203, ecomed, Landsberg/Lech, Germany (1997).